Applicable Analysis
Vol. 91, No. 4, April 2012, 773–786

Taylor & Francis
Taylor & Francis Group

Numerical methods for the shape reconstruction of electrical anomalies using single or double boundary measurements

Kyoungsun Kim and June-Yub Lee*

Department of Mathematics, Institute of Mathematical Sciences, Ewha Womans University, Seoul 120-750, Korea

Communicated by Y.C. Hon

(*Received 28 February 2011; final version received 26 July 2011*)

A solution of the conductivity problem with anomalies of piecewise constant conductivities in a homogeneous medium can be represented as a single layer potential. We propose a simple disk reconstruction method based on the Laurent expansion of the single layer potential to estimate anomalies that can be used as an initial guess for an iterative searching algorithm. Using a simple linear relationship between the normal domain perturbation distance and the boundary perturbation, we develop an iterative algorithm to find anomalies within the domain. The performance of the algorithm is illustrated via numerical examples. The iterative searching algorithm works well in many cases using a single boundary measurement. However, some features of the anomalies require that the algorithm utilize multiple measurements. We discuss the limitations of the inverse conductivity problem using a single Cauchy data set and present a modified version of the algorithm for use with double boundary measurements. The improved performance of this modified numerical scheme is also illustrated with various examples.

Keywords: inverse problem; electrical impedance tomography; Cauchy boundary data

AMS Subject Classifications: 65N21; 65R32; 35R30

1. Introduction

Electrical impedance tomography (EIT), or the inverse conductivity problem (ICP), is a methodology to recover interior conductivity information from boundary measurements of current and potential voltage. The ICP is one of the most important and classical inverse problems, and has applications in many areas of science, engineering and medical imaging. (see [1] and references therein for further details). Our goal in this article is to present a numerical method which finds electrical anomalies sitting inside of a homogenous medium using single or double boundary measurements.

*Corresponding author. Email: jyllee@ewha.ac.kr

ISSN 0003–6811 print/ISSN 1563–504X online

http://dx.doi.org/10.1080/00036811.2011.609814
http://www.tandfonline.com

Let Ω be a bounded simply-connected domain in $\mathbb{R}^2$ with a $C^{2,1}$ boundary and $\{\Omega_i\}_{i=1}^I$ be subsets of Ω that are also bounded and simply-connected with $C^{2,1}$ boundaries. Also suppose that there is a constant d_0 such that $\text{dist}(\Omega_i, \Omega_j) > d_0$ for $i \neq j$, and $\text{dist}(\partial\Omega, \Omega_i) > d_0$ for all i. For a given piecewise conductivity

$$\gamma(\mathbf{x}) = \begin{cases} \gamma_i & \text{if } \mathbf{x} \in \Omega_i \\ \gamma_0 & \text{if } \mathbf{x} \in \Omega_0 = \Omega \setminus \overline{\cup_{i=1}^I \Omega_i} \end{cases}, \tag{1.1}$$

let $u(\mathbf{x})$ be a solution of the conductivity problem

$$\nabla \cdot (\gamma(\mathbf{x}) \nabla u(\mathbf{x})) = 0 \quad \text{in } \mathbf{x} \in \Omega \tag{1.2}$$

which satisfies the continuity condition and the flux jump condition on each of the inclusion boundaries

$$u_i = u_0 \quad \text{and} \quad \gamma_i \frac{\partial}{\partial \nu} u_i = \gamma_0 \frac{\partial}{\partial \nu} u_0 \quad \text{on } \partial\Omega_i \tag{1.3}$$

and also satisfies the Neumann boundary condition $g \in H^{-1/2}(\partial\Omega)$ with $\int_{\partial\Omega} g = 0$,

$$\frac{\partial}{\partial \nu} u = g \quad \text{on } \partial\Omega \tag{1.4}$$

where ν denotes the outward normal direction along the boundaries.

Since $u(\mathbf{x})$ is harmonic in each Ω_i of the anomalies $D := \cup_{i=1}^I \Omega_i$ and in the homogeneous medium $\Omega_0 := \Omega \setminus \overline{D}$, it can be represented as a single layer potential with charge density σ_D on ∂D and a harmonic function $\phi(\mathbf{x})$,

$$u(\mathbf{x}) = \int_{\partial D} G(\mathbf{x}, \mathbf{y}_s) \sigma_D(s) \mathrm{d}s + \phi(\mathbf{x}) \quad \text{for } \mathbf{x} \in \Omega,\ \mathbf{y}_s \in \partial D,$$

where s is a parameterization of the boundary in arclength, $\sigma_D(s)$ is the charge density at $\mathbf{y}_s \in \partial D$, $G(\mathbf{x}, \mathbf{y}) = \frac{1}{2\pi} \log|\mathbf{x} - \mathbf{y}|$ is the Green's function for the two-dimensional Laplacian operator and $\phi(\mathbf{x})$ is a harmonic function that matches the boundary condition.

In Section 2, we propose a simple disk reconstruction method based on the Laurent expansion of the single layer potential $S_D \sigma_D$ which can be directly obtained from a single boundary measurement of Neumann $g(\mathbf{x})$ and the corresponding Dirichlet $\Lambda(g)(\mathbf{x}) := u(\mathbf{x})$ data pair. We numerically demonstrate that the method described in Section 3 could be used as an initial guess for the following iterative searching algorithm.

Suppose Ω_i^* is a ϵ-perturbation of Ω_i^p, that is,

$$\partial\Omega_i^* = \{\mathbf{y}_s + \varepsilon h_i(\mathbf{y}_s) \nu_i(\mathbf{y}_s) : \mathbf{y}_s \in \partial\Omega_i^p\},$$

where ν_i denotes the outward normal vector on $\partial\Omega_i^p$. Shape deformation of $D = \cup_{i=1}^I \Omega_i$ causes a boundary perturbation, a perturbation of modal parameters, etc. The formula presented in Section 4 relates the perturbation distance h_i and $(\Lambda^* - \Lambda^p)(g)$, where Λ^* and Λ^p are the Neumann-to-Dirichlet maps which correspond to the domains with anomalies $\cup_{i=1}^I \Omega_i^*$ and $\cup_{i=1}^I \Omega_i^p$, respectively.

For any given μ in $H^{-1/2}(\partial\Omega)$ and corresponding solution $v(\mathbf{x})$, we can say

$$\gamma_0 \int_{\partial\Omega} \mu(\mathbf{x}_t)\Big(\Lambda^* - \Lambda^p\Big)(g)(\mathbf{x}_t)\mathrm{d}t \approx \varepsilon \sum_{i=1}^{I}(\gamma_0 - \gamma_i)\int_{\partial\Omega_i^p} h_i(\mathbf{y}_s)\Big\{\frac{\partial u^*}{\partial\tau_i}\frac{\partial v}{\partial\tau_i} + \frac{\gamma_0}{\gamma_i}\frac{\partial u^*}{\partial\nu_i}\frac{\partial v}{\partial\nu_i}\Big\}\mathrm{d}s,$$

where t is a parameterization of $\partial\Omega$ in arclength, $\mathbf{x}_t$ is a point on $\partial\Omega$, $\frac{\partial}{\partial\tau_i}$ denotes the tangential derivatives on $\partial\Omega_i^p$ and $u^* = \Lambda^*(g)$. This formula is linear with respect to a normal domain perturbation distance $h_i(\mathbf{y}_s)$, thus can be easily used to find a best updated domain Ω_i^*, in the sense that $\Lambda^*(g)$ matches the given Dirichlet data $f = \Lambda(g)$. It is useful to note that there exist other possible reconstruction algorithms using the polarization tensor (PT) which contain physical and geometric information about the inclusions. Ammari et al. [2] apply an iterative algorithm based on the PT for the reconstruction of a perturbed domain. For details, we refer the readers to [3–5] and the references therein.

In this article, we develop an iterative searching algorithm to find anomalies in the domain based on the linear relationship between the perturbation distance function and the boundary perturbation. In Section 4, we develop an iterative algorithm to find the anomalies in the domain and demonstrate its feasibility using numerical examples. The algorithm works well in many cases including cases with a single boundary measurement. However, some features of the anomalies cannot be recovered using a single measurement. We discuss the limitations of inverse conductivity problem using a single Cauchy data set and present a modified version of the algorithm for use double boundary measurements. The improved performance of this new numerical scheme has been illustrated with various numerical examples in Section 5.

2. A representation formula and a disk searching algorithm

Since potential u is harmonic in each of the inclusions Ω_i and u continuous across the boundaries, u can be represented as a sum of a harmonic function ϕ and a single layer potential with charge density σ_D defined along ∂D,

$$u(\mathbf{x}) = \int_{\partial D} G(\mathbf{x}, \mathbf{y}_s)\sigma_D(s)\mathrm{d}s + \phi(\mathbf{x}). \tag{2.1}$$

Due to the uniqueness of the piecewise conductivity problem (1.2)–(1.4), it is trivial to show that there exists a unique decomposition of u into a sum of a single layer potential $S_D\sigma_D$ and a harmonic function ϕ although there are several possible representations of ϕ depending on the boundary type.

Since any harmonic function $\phi(\mathbf{x})$ in Ω can be written in the form of a single layer potential on $\partial\Omega$, $\phi(\mathbf{x}) = \int_{\partial\Omega} G(\mathbf{x}, \mathbf{y}_s)\sigma_\Omega(s)\mathrm{d}s$, the forward piecewise conductivity solution $u(\mathbf{x})$ with Neumann data g on $\partial\Omega$ can be written in the following form with a single layer density $\sigma(s)$ defined on $\Gamma := \partial D \cup \partial\Omega$,

$$u(\mathbf{x}) = \int_{\Gamma} G(\mathbf{x}, \mathbf{y}_s)\sigma(s)\mathrm{d}s.$$

In order to satisfy the flux continuity condition across the boundary of the i-th inclusion, $\gamma_i \frac{\partial}{\partial \nu} u_i = \gamma_0 \frac{\partial}{\partial \nu} u_0$ and the Neumann boundary condition g on $\partial\Omega$, σ must satisfy the following system of integral equations:

$$\frac{1}{2}\sigma(t) + \lambda_i \int_\Gamma \frac{\partial}{\partial \nu_{\mathbf{x}}} G(\mathbf{x}(t), \mathbf{y}_s)\sigma(s)\mathrm{d}s = 0 \quad \text{on } \mathbf{x}(t) \in \partial\Omega_i,\ i = 1, \ldots, I \tag{2.2}$$

and

$$-\frac{1}{2}\sigma(t) + \int_\Gamma \frac{\partial}{\partial \nu_{\mathbf{x}}} G(\mathbf{x}(t), \mathbf{y}_s)\sigma(s)\mathrm{d}s = g(t) \quad \text{on } \mathbf{x}(t) \in \partial\Omega, \tag{2.3}$$

where $\lambda_i = \frac{\gamma_0 - \gamma_i}{\gamma_0 + \gamma_i}$ and $\frac{\partial}{\partial \nu_{\mathbf{x}}}$ denotes the normal derivative with respect to $\mathbf{x}$.

Suppose we have an over-determined but consistent Cauchy data pair $g = \frac{\partial u}{\partial \nu}\big|_{\partial\Omega}$ and $f = u|_{\partial\Omega}$ along the boundary $\partial\Omega$. Then a piecewise harmonic function $v(\mathbf{x})$ defined as $v(\mathbf{x}) := u(\mathbf{x})$, $\mathbf{x} \in \Omega$ and $v(\mathbf{x}) := 0$, $\mathbf{x} \in \mathbb{R}^2 \backslash \Omega$ can be written in the form of $v(\mathbf{x}) = S_D\psi_D(\mathbf{x}) + S_\Omega g(\mathbf{x}) - D_\Omega f(\mathbf{x})$ where

$$S_\Omega g(\mathbf{x}) = \int_{\partial\Omega} G(\mathbf{x}, \mathbf{y}_s)\, g(s)\mathrm{d}s, \quad D_\Omega f(\mathbf{x}) = \int_{\partial\Omega} \frac{\partial}{\partial \nu_{\mathbf{y}}} G(\mathbf{x}, \mathbf{y}_s) f(s)\mathrm{d}s.$$

Since $u(\mathbf{x}) \equiv v(\mathbf{x})$ for $\mathbf{x} \in \Omega$ and the piecewise conductivity problem has a unique solution, it is trivial to show that $\sigma_D(s) = \psi_D(s)$, $\mathbf{y}_s \in \partial D$ and $\phi(\mathbf{x}) = S_\Omega g(\mathbf{x}) - D_\Omega f(\mathbf{x})$, $\mathbf{x} \in \Omega$. Therefore, $u(\mathbf{x})$ can be written as a combination of a single layer potential along the boundaries of the inclusions and a sum of a single and double layer potential along the boundary of the domain,

$$u(\mathbf{x}) = \int_{\partial D} G(\mathbf{x}, \mathbf{y}_s)\sigma_D(s)\mathrm{d}s + S_\Omega g(\mathbf{x}) - D_\Omega f(\mathbf{x}), \quad \mathbf{x} \in \Omega, \tag{2.4}$$

where σ_D is a solution of the system of integral equations (2.2)–(2.3). It is not surprising that the harmonic function $\phi(\mathbf{x})$ written as a sum of a single and a double layer potential appears frequently in the inverse conductivity problem [6–8] since it contains all the information regarding the interior of the inclusions. Before we present a new disk searching scheme, it is useful to note that there exist many algorithms which utilize this representation directly in this form or in some other form. However, many of these methods require a sequence of forward solvers (e.g. [9]) while our method described below does not. Additionally, there are other reconstruction methods [10–12] which do not use a forward solver, but are relatively complicated as compared to the algorithm of this article.

Since $u(\mathbf{x})$ in (2.4) is identical to zero in $\mathbb{R}^2 \setminus \Omega$, $S_D\sigma_D$ can be represented [13,14] as layer potentials induced by f and g,

$$S_D\sigma_D(\mathbf{x}) = D_\Omega f(\mathbf{x}) - S_\Omega g(\mathbf{x}), \quad \mathbf{x} \in \mathbb{R}^2 \setminus \Omega. \tag{2.5}$$

We now extend the definition of the single and double layer potentials to complex-valued functions. Suppose $z \in \mathbb{C}$ corresponds to $\mathbf{x} \in \mathbb{R}^2$ and $\xi(s)$ to $\mathbf{y}_s \in \partial D$, then the complex valued single layer potential $S_D\sigma_D(z)$ is defined as follows:

$$S_D\sigma_D(z) = \frac{1}{2\pi} \int_{\partial D} \log(z - \xi(s))\sigma_D(s)\mathrm{d}s. \tag{2.6}$$

Here the integral is well defined regardless of the branch cuts of $\log(z-\xi(s))$, which are assigned independently for each component Ω_i since $\int_{\partial\Omega_i}\sigma_D(s)\mathrm{d}s=0$ (see [15,16] and references therein for more details about the properties of the system of the integral equations (2.2)–(2.3)). The complex-valued double layer can be defined similarly, and the solution of the piecewise conductivity problem $u(z)$ is the real part of $w(z):=S_D\sigma_D(z)+S_\Omega g(z)-D_\Omega f(z)$.

Since $S_D\sigma_D(z)$ has singularities only along ∂D, it can be written in terms of a Laurent expansion centred at z_0 for $|z-z_0|\geq R_D(z_0):=\max_{\xi\in\partial D}|\xi-z_0|$,

$$\begin{aligned}S_D\sigma_D(z)&=\frac{1}{2\pi}\int_{\partial D}\log(z-\xi(s))\sigma_D(s)\mathrm{d}s\\&=\frac{1}{2\pi}\int_{\partial D}\left\{\log(z-z_0)+\log\left(1-\frac{\xi(s)-z_0}{z-z_0}\right)\right\}\sigma_D(s)\mathrm{d}s\\&=\frac{\log(z-z_0)}{2\pi}\int_{\partial D}\sigma_D(s)\mathrm{d}s-\frac{1}{2\pi}\int_{\partial D}\sum_{n=1}^{\infty}\frac{1}{n}\left(\frac{\xi(s)-z_0}{z-z_0}\right)^n\sigma_D(s)\mathrm{d}s.\end{aligned}$$

Therefore,

$$S_D\sigma_D(z)=\sum_{n=1}^{\infty}\frac{a_n^{z_0}}{(z-z_0)^n},\quad a_n^{z_0}=\frac{-1}{2\pi n}\int_{\partial D}(\xi(s)-z_0)^n\sigma_D(s)\mathrm{d}s. \tag{2.7}$$

Note that $\left|a_n^{z_0}\right|\leq C\cdot(R_D(z_0))^n$ and $R_D(z_0)\geq\liminf_{n\to\infty}\left|a_n^{z_0}\right|^{1/n}$.

On the other hand, the Laurent expansion $\{a_n^{z_0}\}$ of the boundary layer potentials

$$D_\Omega f(z)-S_\Omega g(z)=\sum_{n=1}^{\infty}\frac{a_n^{z_0}}{(z-z_0)^n},\quad |z-z_0|\geq R_\Omega(z_0) \tag{2.8}$$

centred at z_0 is easily computable from the Cauchy data pair (f,g) as follows:

$$a_n^{z_0}=\frac{1}{2\pi n}\int_{\partial\Omega}(\xi(t)-z_0)^n g(t)\mathrm{d}t-\frac{1}{2\pi}\int_{\partial\Omega}(\xi(t)-z_0)^{n-1}\nu_t f(t)\mathrm{d}t, \tag{2.9}$$

where $\xi(t)$ is a point on $\partial\Omega$ and ν_t is a unit normal vector at $\xi(t)$ in complex value notation.

Suppose the Laurent expansion $\{a_n^{z_0}\}$ of $S_D\sigma_D$ centred at an arbitrary point z_0 is given via the formula (2.9) from a single boundary measurement (f,g). For a fixed point z_0, we define the effective radius

$$R_{\mathrm{eff}}(z_0):=\left|\frac{a_{n+m}^{z_0}}{a_n^{z_0}}\right|^{\frac{1}{m}} \tag{2.10}$$

for some n, m such that $|a_n|\gg|a_{n+m}|\gg 0$. The following linear regression formula gives a slightly better approximation:

$$R_{\mathrm{eff}}(z_0):=\exp\left(\frac{\sum' p\log|a_p|-\sum' p\sum'\log|a_p|}{\sum' p^2-(\sum' p)^2}\right), \tag{2.11}$$

where $\sum'$ denotes the average over $p = n, n+1, \ldots, n+m$. It is easy to recompute the Laurent expansion when the centre of the expansion is shifted to z_1,

$$a_n^{z_1} := \sum_{m=1}^{n} {}_nC_m (z_0 - z_1)^m a_{n-m}^{z_0}. \tag{2.12}$$

A simple disk reconstruction algorithm is used to find a disk with a centre z_c and smallest corresponding effective radius $R_{\text{eff}}(z_c)$ such that

$$z_c := \operatorname*{argmin}_{z \in \Omega} R_{\text{eff}}(z). \tag{2.13}$$

3. Numerical examples of the disk reconstruction method

We have implemented a forward solver based on the system of integral equation (2.2)–(2.3). The integral equations were discretized using the equispaced trapezoidal rule along the boundaries, which guarantees super-algebraic convergence. We set the number of discretization points along each of the boundaries to range between 64 and 256. Under these conditions, a GMRES-type solver usually provided a solution with relative error smaller than 10^{-10} after 10–30 iterations.

Example 1 The first examples contains a conductive inclusion ($\gamma_1/\gamma_0 = 10^2$) with 5-leaves. Figure 1 shows the computational domain and the decay rates of $|a_n(z_0)|$ depending on z_0. We choose $|a_n(z_0)|$ to be greater than 10^{-3} and $|a_{n+m}(z_0)|$ to be less than 10^{-9} to compute the effective radius using (2.11). The left figure shows that the effective radius is $R_{\text{eff}} \approx 0.28$ for $z_0 \approx (-0.05, -0.05)$. As z_0 approaches the centre of the inclusion, the decay rate of $|a_n(z_0)|$ becomes stiffer and the effective radius reaches its minimum value of $R_{\text{eff}} \approx 0.095$ near $z_c \approx (0.1, 0.1)$. Contour lines outside of the effective disks represent the potential generated by the Laurent expansion in (2.8).

Example 2 In order to test the numerical robustness of the algorithm, we add random noise to the Cauchy boundary data (g, f). Both additive noise $w_a(t)\|g\|_{\partial\Omega}$ and multiplicative noise $g(t)w_m(t)$ are added to $g(t)$, where w_a, w_m are independent

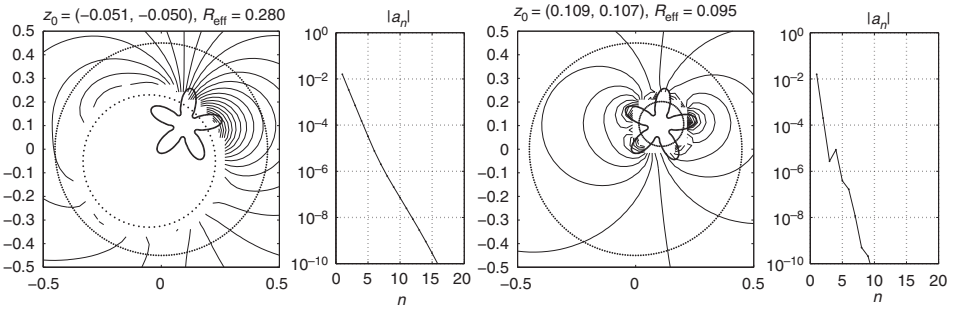

Figure 1. Decay rate of multipole expansion $a_n(z_0)$.

random variables with uniform distribution on $(-1,1)\times Noise_{Level}$. Similarly, random noises of $Noise_{Level}$ also modify the Dirichlet potential $f(t)$.

The leftmost figure in Figure 2 shows the computational result for a fixed $z_0=(0.075,0.0)$ without any noise added. The middle plots shows the decay rate of $|a_n(z_0)|$ depending on the noise level, $Noise_{Level}=0,10^{-3},10^{-1}$. We observe that the decay rate is relatively constant when there is no noise. However, higher frequency modes with small modulus are prone to error. It is possible to find an optimal range of a_n and a_{n+m} by comparing (g,f) and the Laurent expansion of (2.8), especially for high noise cases, although, we simply reduced the number of modes used by restricting $|a_{n+m}(z_0)|<5\times10^{-6}$.

The rightmost figure numerically demonstrates that the error of effective radius is linearly proportional to the noise level. It is worth mentioning that despite the extreme ill-conditioning of the electrical impedance tomography problem [17], the process of finding the effective radius and the corresponding centre of a disk is a relatively stable algorithm since it requires only the first few modes of a_n which are less prone to noise [18].

Example 3 We implemented the disk minimization algorithm (2.13) using the subplex (subspace-searching simplex method) package by Rowan [19]. Figure 3 shows the computational results in dotted lines for three different cases, starting with a initial

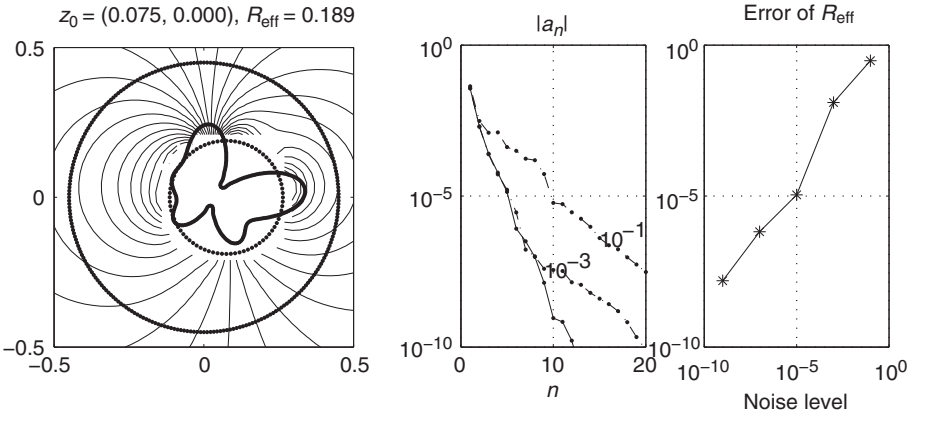

Figure 2. Effective rate under noisy situation.

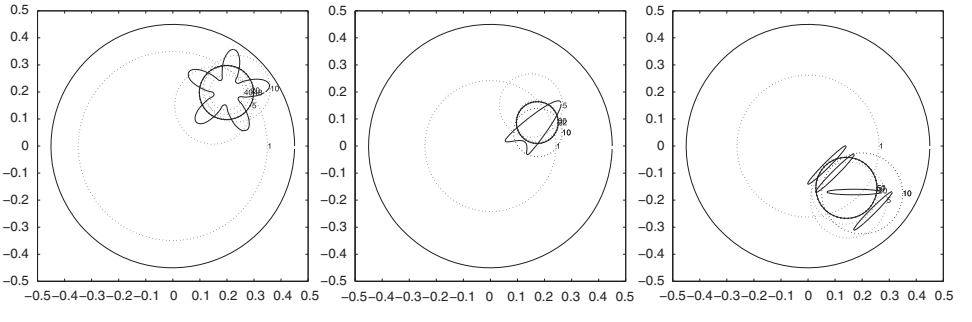

Figure 3. Disk search algorithm.

guess at $z_0 = (0, 0)$. The final results are drawn in dark lines. The conductivity of the background media is 1, the star shape inclusion is 10^2, the kite is 10^{-3} and the four inclusions in the rightmost figures are 10^{-2}, 10^{-1}, 10^1, 10^2 from centre to boundary.

We have proven that there exists at least one interface point outside of the constructed disk. Also, we observe that the disk searching algorithm usually gives good approximations of the actual size and geometric centre of the inclusions. However, there is no guarantee that this is always true. We know that a smooth inclusion in a linear field does not generate higher frequency modes, thus the effective radius is smaller than the actual size of the domain. A noticeable example is in the case of a disk in a uniform gradient field, which has no multipole moments higher than a dipole, and thus gives an effective radius of zero.

4. Reconstruction method using a single measurement

We start this section with a comment on the linear relationship between the domain perturbation and the boundary perturbation. There exist many attempts to find a relationship between a small perturbation of the domain and the corresponding N-to-D map. One of the most notable improvements was derived by Ammari–Kang et al. (see [2] and references therein). For example, it is derived in [2] that the asymptotic formula for the eigenvalue due to the changes of the shape of the inclusions. They also derived the asymptotic equation for the perturbation and the N-to-D map as a dual formula. Ammari–Kang–Lim–Zribi developed a formula for the inverse conductivity problem and used it for the reconstruction of the conductive inclusions [4]. The following formula is also based on the same relation, and our goal in this article is to develop a robust numerical method by studying the numerical conditioning of the linear system derived from it.

Let us consider a perturbed domain Ω_i^* of a given domain Ω_i^p for $i = 1, \ldots, I$,

$$\partial\Omega_i^* = \{\mathbf{y}_s + \varepsilon h_i(\mathbf{y}_s)\nu_i(\mathbf{y}_s) \,|\, \mathbf{y}_s \in \partial\Omega_i^p\},$$

where $\nu_i(\mathbf{y}_s)$ is the outward unit normal to the interfaces at $\mathbf{y}_s \in \partial\Omega_i^p$ and $h_i \in C^{1,1}(\partial\Omega_i^p)$ with $||h_i||_{C^{1,1}(\partial\Omega_i^p)} < \infty$. Suppose that the conductivity profiles γ and γ^* in Ω are given by (1.1) and

$$\gamma^*(\mathbf{x}) = \begin{cases} \gamma_i & \text{if } \mathbf{x} \in \Omega_i^* \\ \gamma_0 & \text{if } \mathbf{x} \in \Omega \setminus \overline{\cup_{i=1}^I \Omega_i^*}. \end{cases} \tag{4.1}$$

Then, the integral equation in the following theorem relates a domain perturbation $h_i(\mathbf{y}_s)$, $\mathbf{y}_s \in \partial\Omega_i^p$ and a perturbation of the Dirichlet data $u(\mathbf{x})$ on the boundary $\partial\Omega$.

LEMMA 4.1 *Let $u^* = \Lambda^*(g)$, $u^p = \Lambda^p(g)$ for a given $g \in H^{-1/2}(\partial\Omega)$ with $\int_{\partial\Omega} g = 0$. For any given Neumann boundary function $\mu \in H^{-1/2}(\partial\Omega)$ and the corresponding conductivity solution $v = \Lambda^p(\mu)$, we have*

$$\begin{aligned} &\int_{\partial\Omega} \gamma_0 \mu(\mathbf{x}_t)\Big(\Lambda^* - \Lambda^p\Big)(g)(\mathbf{x}_t)\mathrm{d}t \\ &\quad = \varepsilon \sum_{i=1}^{I} (\gamma_0 - \gamma_i) \int_{\partial\Omega_i^p} h_i(\mathbf{y}_s)\left\{ \frac{\partial u^p}{\partial \tau_i}\frac{\partial v}{\partial \tau_i} + \frac{\gamma_0}{\gamma_i}\frac{\partial u^p}{\partial \nu_i}\frac{\partial v}{\partial \nu_i} \right\}(\mathbf{y}_s)\mathrm{d}s + O(\varepsilon^{1+\beta}) \end{aligned} \tag{4.2}$$

for some $\beta > 0$, where τ_i is the tangent vector to $\partial\Omega_i^p$.

Proof We omit a proof in this article, but note that the proof of this Lemma is identical to that of the asymptotic formula in [2]. The above integral equation and its derivation can be found in [4].

We now present an iterative domain searching algorithm based on the linear relationship between $(\Lambda^* - \Lambda^p)(g)$ and h_i in (4.2). Suppose our unknown target domain is Ω^* and the Cauchy data pair $(g, f = \Lambda^*(g))$ is given on $\partial\Omega$. In order to apply an iterative scheme, we need an initial guess for $\Omega^{p=0}$, and the result of the disk reconstruction method described in Sections 2 and 3 is a good candidate, especially when there is only one inclusion. With the aid of a numerical forward solver on Ω^p, we can compute $(\Lambda^* - \Lambda^p)(g)$ and h_i. Once we compute $\{h_i\}_{i=1}^I$, we may update our domain $\partial\Omega_i^{p+1} = \{\mathbf{y}_s + \varepsilon h_i(\mathbf{y}_s)\nu_i(\mathbf{y}_s) \mid \mathbf{y}_s \in \partial\Omega_i^p\}$ until $\|h_i\|$ is smaller than the prescribed tolerance. The following description is a process to update Ω^p to Ω^{p+1}.

Let us choose a function μ_q in $H^{-1/2}(\partial\Omega)$ satisfying $\int_{\partial\Omega} \mu_q = 0$. Then, we can find the corresponding solution $v_q = \Lambda^p(\mu_q)$ by solving the forward problem numerically on Ω^p. We use the following notations:

$$\delta f(\mathbf{x}) = \Big(\Lambda^* - \Lambda^p\Big)(g)(\mathbf{x}) \quad \text{for } \mathbf{x} \in \partial\Omega, \tag{4.3}$$

$$J_q^i(\mathbf{y}) = (\gamma_0 - \gamma_i)\left\{ \frac{\partial u^p}{\partial \tau_i}(\mathbf{y}) \frac{\partial v_q}{\partial \tau_i}(\mathbf{y}) + \frac{\gamma_0}{\gamma_i} \frac{\partial u^p}{\partial \nu_i}(\mathbf{y}) \frac{\partial v_q}{\partial \nu_i}(\mathbf{y}) \right\} \quad \text{for } \mathbf{y} \in \partial\Omega_i. \tag{4.4}$$

Then, the integral equation (4.2) for a single pair of data (v_q, μ_q) reads

$$\begin{pmatrix} C_q^1 & C_q^2 & \cdots & C_q^I \end{pmatrix} \begin{pmatrix} H_1 \\ \vdots \\ H_I \end{pmatrix} = \sum_{a=1}^{A} \gamma_0 \mu_q(\mathbf{x}_a) \delta f(\mathbf{x}_a) \Delta\mathbf{x}, \tag{4.5}$$

where $\Delta\mathbf{x}$ is a distance between two adjacent points among $\mathbf{x}_1, \ldots, \mathbf{x}_A \in \partial\Omega$ and for $\mathbf{y}_i^1, \ldots, \mathbf{y}_i^{B_i} \in \partial\Omega_i$ with spacing $\Delta\mathbf{y}_i$,

$$C_q^i = \begin{pmatrix} J_q^i(\mathbf{y}_i^1) & \cdots & J_q^i(\mathbf{y}_i^{B_i}) \end{pmatrix} \Delta\mathbf{y}_i, \quad H_i = \begin{pmatrix} \varepsilon h_i(\mathbf{y}_i^1) \\ \vdots \\ \varepsilon h_i(\mathbf{y}_i^{B_i}) \end{pmatrix}.$$

Of course, this equation can not be solved since there is only one equation with $\sum_{i=1}^I B_i$ unknowns. Even though we have only one or two boundary measurements for $(g, \delta f)$ on $\partial\Omega$, we may generate arbitrarily many choices for the pairs $(\mu_q, \Lambda^p(\mu_q))$. The integral equation (4.5) with Q different choices for μ_q becomes

$$\begin{pmatrix} C^1 & \cdots & C^I \end{pmatrix} \begin{pmatrix} H_1 \\ \vdots \\ H_I \end{pmatrix} = \mu F, \tag{4.6}$$

where

$$C^i = \begin{pmatrix} J_1^i(\mathbf{y}_i^1) & \cdots & J_1^i(\mathbf{y}_i^{B_i}) \\ \vdots & \ddots & \vdots \\ J_Q^i(\mathbf{y}_i^1) & \cdots & J_Q^i(\mathbf{y}_i^{B_i}) \end{pmatrix} \Delta\mathbf{y}_i, \quad \mu F = \begin{pmatrix} \sum_{a=1}^A \gamma_0 \mu_1(\mathbf{x}_a) \delta f(\mathbf{x}_a) \\ \vdots \\ \sum_{a=1}^A \gamma_0 \mu_Q(\mathbf{x}_a) \delta f(\mathbf{x}_a) \end{pmatrix} \Delta\mathbf{x}.$$

Note that C^i are $Q \times B_i$, H_i are $B_i \times 1$ matrices, and the right-hand side of (4.6) is a $Q \times 1$ matrix. To solve this system of linear equations uniquely, we need more constraints than unknowns, $Q \geq \sum_{i=1}^{I} B_i$. However, increasing Q requires application of more numerical forward solvers for $v_q = \Lambda^p(\mu_q)$ on Ω^p.

Further difficulties arise due to ill-conditioning of the system when the number of discretization points $\sum_{i=1}^{I} B_i$ becomes large. We represent H_i using K-fourier modes $\widehat{H}_i := \{\widehat{h}_i^k\}_{k=0}^{2K}$ to overcome this difficulty,

$$H_i = \begin{pmatrix} h_i(\mathbf{y}_i^1) \\ \vdots \\ h_i(\mathbf{y}_i^{B_i}) \end{pmatrix} = \begin{pmatrix} \widehat{h}_i^0 + \sum_{k=1}^{K} \left\{ \widehat{h}_i^{2k-1} \cos(k\theta^1) + \widehat{h}_i^{2k} \sin(k\theta^1) \right\} \\ \vdots \\ \widehat{h}_i^0 + \sum_{k=1}^{K} \left\{ \widehat{h}_i^{2k-1} \cos(k\theta^{B_i}) + \widehat{h}_i^{2k} \sin(k\theta^{B_i}) \right\} \end{pmatrix}$$
$$= \begin{pmatrix} 1 & \cos(\theta^1) & \cdots & \sin(K\theta^1) \\ \vdots & \vdots & \ddots & \vdots \\ 1 & \cos(\theta^{B_i}) & \cdots & \sin(K\theta^{B_i}) \end{pmatrix} \begin{pmatrix} \widehat{h}_i^0 \\ \vdots \\ \widehat{h}_i^{2K} \end{pmatrix} := \mathcal{F}_i \widehat{H}_i,$$

where $\{\theta^1, \ldots, \theta^{B_i}\} \in [0, 2\pi]$ is a parameterization of $\partial\Omega_i$ corresponding to $\{\mathbf{y}_i^1, \ldots, \mathbf{y}_i^{B_i}\}$. We choose K such that the smallest singular value of the Q-by-$(2K+1)I$ coefficient matrix $M_{Q,K}$ in

$$M_{Q,K} \widehat{H} := \begin{pmatrix} C^1 \mathcal{F}_1 & \cdots & C^I \mathcal{F}_I \end{pmatrix} \begin{pmatrix} \widehat{H}_1 \\ \vdots \\ \widehat{H}_I \end{pmatrix} \tag{4.7}$$

is larger than the error level $\|\delta f\|$. This updating process from the well-conditioned system of linear equations continues until $\|\widehat{H}\|$ is small enough.

Before we give a formal description of the algorithm, it is worth to remarking that this numerical scheme is not based on a non-linear optimization technique. For a given Q, K, the matrix $M_{Q,K}$ in (4.7) is merely a numerical discretization of right-hand side of the integral equation (4.2), and the linear system of equations $M_{Q,K}\widehat{H} = \mu F$ can be solved uniquely in l_2-least squares sense. The numerical method automatically maximizes the number of Fourier modes K under the condition that the singular values of $M_{Q,K}$ are larger than the user specified noise level f_{noise}, therefore, the method is free from user-specified tuning parameters once the number of forward simulations Q and an estimation of the noise level f_{noise} are specified. Following is a formal description of the implementation.

A domain searching algorithm

Step I: Initialization

1. With given $(g, f = \Lambda^*(g))$ on $\partial\Omega$, compute an initial disk $\Omega^{p=0}$ by (2.13).
2. Set number of forward solutions Q, input noise level f_{noise}, update frequency modes $K_{\max}(< Q/2)$ and stop tolerance H_{tol}.

Step U: Update

1. Compute $u^p = \Lambda^p(g)$ on Ω^p.

2. Compute $\{v_q = \Lambda^p(\mu_q)\}_{q=1}^{Q}$ on Ω^p with $\mu_{2q-1} = \cos(q\theta)$, $\mu_{2q} = \sin(q\theta)$.
3. For $K := 1$ to $K_{\max}$,
   Form matrix $M_{Q,K}$ defined in (4.7).
   Compute the smallest singular of $M_{Q,K}$.
   If smallest singular value $< f_{noise}$, break at the previous K.
4. Find $\widehat{H}$ from $M_{Q,K}\widehat{H} = \mu F$ in a least square sense.
5. Set $\partial\Omega_i^{p+1} = \{\mathbf{y}_s + \varepsilon h_i(\mathbf{y}_s)\nu_i(\mathbf{y}_s) \mid \mathbf{y}_s \in \partial\Omega_i^p\}$.

Step T: Termination

1. Stop if $\|\widehat{H}\| < H_{tol}$. Otherwise repeat Step U with new Ω^{p+1}.

5. Numerical results and concluding remarks

We have implemented the domain searching algorithm presented in the previous section in Fortran, and the forward solver described in Section 3 was used to generate the numerical Cauchy boundary data (g, f) and $(\mu_q, v_q = \Lambda(\mu_q))$. We set $Q = 20$ and the maximum frequency mode for $\widehat{H}_i$-updates to be $K_{\max} = 6$. The iteration process continued until the norm of $\widehat{H}$-update was less than $H_{tol} = 5 \times 10^{-3}$. Three numerical examples are given below: one with a single boundary measurement, another with double boundary measurements, and the last with multiple inclusions.

Example 4 The first example contains a single object with a size of about $0.3^2|\Omega|$ near the centre of a circular domain Ω. The conductivity of the inclusion is 100 times higher than the background. The Cauchy data pair $g = \cos(\theta)$ and $f = \Lambda(g)$ on the boundary $\partial\Omega$ is given by the numerical forward solver. In Figure 4, the solid line shows the target domain and the dotted lines represent computed domains Ω^p for $p = 1, \ldots, 5$. In each iteration, we choose the number of the update frequency modes K such that the smallest singular value of $M_{q,K}$ is greater than $0.1 \times \|f - \Lambda^p(g)\|_{\partial\Omega}$. The results show that K was chosen to be 4 for the first three iterations where the discrepancy of the boundary Dirichlet data is relatively large, and the iteration converges at $p = 5$ with $K = 6$.

We numerically tested the algorithm with various examples, and it performed well in most cases, however, sometimes gave less satisfactory results. The following example shows the limitations of the scheme, and a fix to improve convergence under certain conditions.

Example 5 We set the numerical parameters to be the same as in the previous example, and the upper plots in Figure 5 are the reconstructed domains using a single

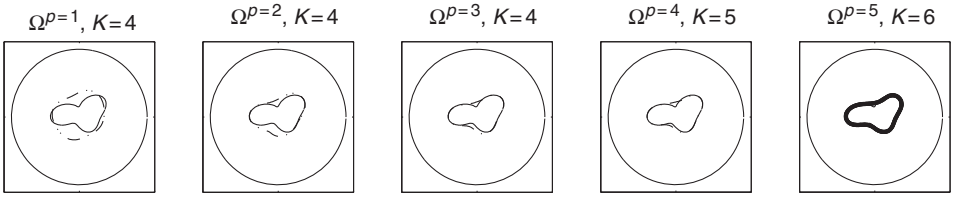

Figure 4. Star-shaped inclusion with a single-boundary measurement.

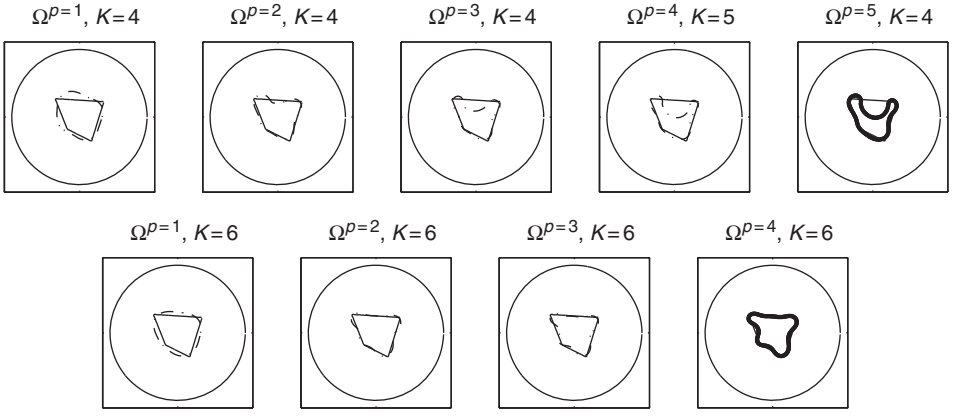

Figure 5. Reconstruction with single and double boundary measurements. Top plots using a single Cauchy datum, Bottom plots using two Cauchy data.

current and voltage pair. The reconstruction method gives a good approximation of the inclusion after just two iterations, however, large errors on the top edge emerge as the iteration continues.

This phenomenon is usually observed when a large edge of an inclusion is parallel to the current flow direction, left-to-right in this example. Moving an edge parallel to the current flow direction generates much smaller perturbation than a perpendicular edge movement which makes no changes to the current but causes large changes in the potential. This symptom is not particular to this algorithm, but rather common in many inverse conductivity reconstruction methods which use only one boundary Neumann-to-Dirichlet map. A common cure is to use double measurements with internal currents flowing relatively orthogonal to each other.

We use two boundary measurements, the first ($g = \cos\theta$, $f = \Lambda(g)$) with current mainly flows from left to right and another ($g_2 = \sin\theta$, $f_2 = \Lambda(g_2)$) with current flowing from bottom to top. The only modification of the algorithm is that we solve (4.6) in a least square sense simultaneously with two right-hand sides, μF and μF_2. Bottom plots in Figure 5 show the reconstruction results. Since we use only limited frequency modes to update the interface, sharp corners are not captured when using a single measurement. However, the final reconstruction matches with all four edges correctly.

Example 6 The last example contains two inclusions. In general, it is difficult to find a good initial guess for multiple inclusions or to develop an automatic domain separation (or topology updating) method. In this example, we assume that an initial guess is known consisting of multiple disks. Figure 6 shows the initial disks and updated domains in dotted lines, and the target domains in solid lines. This numerically demonstrates that the update procedure works very well even in the presence of multiple inclusions, as long as the inclusions are well separated by the initial guesses.

In summary, we have developed a disk searching method based on the decay rate of the multipole expansion of the Cauchy boundary data, which requires no forward

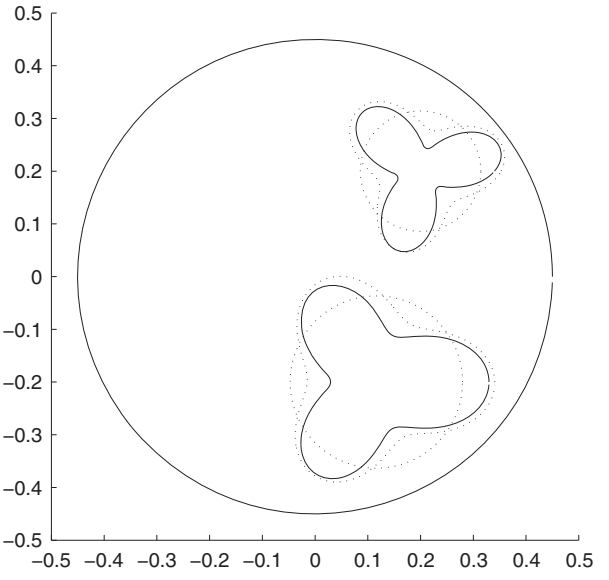

Figure 6. Reconstruction with multiple inclusions.

solver. Using an initial guess and double boundary measurements, our domain update algorithm is able to correctly recover inclusion edges which are parallel to current flow using a moderate number of Fourier modes $\widehat{H}_i$. The exact number of Fourier modes needed depends on the noise level and the convergence error $(\Lambda - \Lambda^p)(g)(x)$. More studies are needed to build an automatic optimal parameter tuner for robust updates and a numerical scheme for automatically splitting one object into multiple components.

Acknowledgements

We thank two anonymous referees for their valuable comments and suggestions on an earlier version of this article. Their suggestions have helped us to make this article more concise and easily readable. The work by J.-Y. Lee was supported in part by the Priority Research Centers Program from National Research Foundation of Korea, NRF-2010-0028298.

References

[1] M. Cheney, D. Isaacsony, and J. Newell, *Lectrical impedance tomography*, SIAM Rev. 41(1) (1999), pp. 85–101.

[2] H. Ammari, E. Beretta, E. Francini, H. Kang, and M. Lim, *Optimization algorithm for reconstructing interface changes of a conductivity inclusion from modal measurements*, Math. Comp. 79 (2010), pp. 1757–1777.

[3] H. Ammari and H. Kang, *Reconstruction of Small Inhomogeities from Boundary Measurements*, Lecture Notes in Mathematics, Vol. 1846, Springer-Verlag, Berlin, 2004.

[4] H. Ammari, H. Kang, M. Lim, and H. Zribi, *The generalized Polarization Tensors for resolved imaging. Part I: Shape reconstruction of a conductivity inclusion*, Math. Comp. (to appear).
[5] H. Ammari, H. Kang, E. Kim, and J.-Y. Lee, *The generalized polarization tensors for resolved imaging. Part II: Shape and electromagnetic parameters reconstruction of an electromagnetic measurements*, Math. Comp. (to appear).
[6] H. Eckel and R. Kress, *Non-linear integral equations for the complete electrode model in inverse impedance tomography*, Appl. Anal. 87 (2008), pp. 1267–1288.
[7] E. Fabes, H. Kang, and J.K. Seo, *Inverse conductivity problem with one measurement: Error estimates and approximate identification for perturbed disks*, SIAM J. Math. Anal. 30(4) (1999), pp. 699–720.
[8] H. Kang, J.K. Seo, and D. Sheen, *The inverse conductivity problem with one measurement: Stability and estimation of size*, SIAM J. Math. Anal. 28(6) (1997), pp. 1389–1405.
[9] H. Ki and D. Sheen, *Numerical inversion of discontinuous conductivities*, Inv. Probl. 16 (2000), pp. 33–47.
[10] M. Hanke, *On real-time algorithms for the location search of discontinuous conductivities with one measurement*, Inv. Probl. 24 (2008), p. 045005.
[11] O. Kwon and J.K. Seo, *Total size estimation and identification of multiple anomalies in the inverse conductivity problem*, Inv. Probl. 17 (2001), pp. 59–75.
[12] O. Kwon, J.K. Seo, and J.-R. Yoon, *A real-time algorithm for the location search of discontinuous conductivities with one measurement*, Commun. Pure Appl. Math. 55 (2002), pp. 1–29.
[13] H. Kang and J.K. Seo, *Layer potential technique for the inverse conductivity problem*, Inv. Probl. 12 (1996), pp. 267–278.
[14] H. Kang and J.K. Seo, *Recent progress in the inverse conductivity problem with single measurement*, in *Inverse Problems and Related Fields*, G. Nakamura, S. Saitoh, J.K. Seo, and M. Yamamoto, eds., CRC Press, Boca Raton, FL, 2000, pp. 69–80.
[15] A. Greenbaum, L. Greengard, and G.B. McFadden, *Laplace's equation and the Dirichlet–Neumann map in multiply connected domains*, J. Comput. Phys. 105(2) (1993), pp. 267–278.
[16] L. Greengard and J.-Y. Lee, *Electrostatics and heat conduction in high contrast composite materials*, J. Comput. Phys. 211(1) (2006), pp. 64–76.
[17] S. Nagayasu, G. Uhlmann, and J.-N. Wang, *A depth-dependent stability estimate in electrical impedance tomography*, Inv. Probl. 25 (2009), p. 075001.
[18] J.-Y. Lee and J.-R. Yoon, *A numerical method for cauchy problem using singular value decomposition Comm*, Korean Math. Soc. 16(3) (2001), pp. 487–508.
[19] T. Rowan, *Functional stability analysis of numerical algorithms*, Ph.D. thesis, Department of Computer Sciences, University of Texas at Austin, 1990.